

Capillary Flow of Carbon Dioxide – Water Emulsions

Brian Quinn*, Pradnya Bhagwat, David Krank

Aktiv-Dry LLC, 6060 Spine Road, Boulder, CO, USA
*Corresponding author: Brian Quinn, bquinn@aktiv-dry.com

This paper describes experiments in which high pressure emulsions, formed by mixing supercritical, or near-critical, carbon dioxide and water, flow through capillaries. Motivation for the work is found in a process for making nano- and micro-particulate powders by expanding similarly formed emulsions of solvent systems through small-diameter flow restrictors to atmospheric pressure. The expansion acts to nebulize the solution or suspension of a compound (usually pharmaceutical) and form a plume of small droplets and bubbles. Applying heat to the plume evaporates the solvent and leaves behind the particles ready for collection. Particle size and morphology are controlled by adjusting the operating pressures and temperatures, and by adjusting the flow rates of the solution and the carbon dioxide. It has been shown in other work that the ratio of the two fluid flow rates is a key factor in engineering particle size and morphology. Unfortunately, equipment operators have no means for knowing, *à priori*, what the value of the ratio will be for a given pressure and restrictor geometry.

To shed light on the problem, experiments were completed with a family of silica glass capillaries whose lengths spanned 5 to 25 cm and whose internal diameters varied between 75 and 200 microns. The resulting length – diameter ratios were in the range $660 \leq L/D \leq 2000$, approximately. Pressures were set incrementally between 7 and 14 MPa and most experiments were completed at room temperature, around 20 °C. The two-species system is complex. In general, for given pressure and temperature at the capillary inlet, the flux of carbon dioxide decreases as the flux of water increases. But this general trend appears to be only piecewise continuous and defined by two distinct branches, an upper and a lower on a CO₂ flow rate vs H₂O flow rate diagram. On the upper branch, the CO₂ flow rate decreases moderately until the increasing H₂O flow rate reaches a threshold value, on the order of 1 or 2 ml/min. At the threshold water flow rate, the CO₂ flow rate drops precipitously to the lower branch where it has been observed to remain — or to oscillate between the two branches. The upper branch appears to relate to a water-in-carbon dioxide emulsion while the lower branch is a carbon dioxide-in-water emulsion.

INTRODUCTION

A new and relatively simple process for making nano- and micro-scale powders uses capillary flow restrictors to nebulize solutions of commercial interest. The process, called CAN-BD [1], expands a mixture of a high pressure solution, or suspension, and critical or near-critical carbon dioxide to ambient pressure thereby forming what appears to be a plume of very small bubbles and droplets (Figure 1). Directing the plume into a drying chamber through which heated nitrogen is flowing evaporates the liquid phases and reduces the solute to the desired small particles that are then collected on a filter or other harvesting device. The solutions may consist of aqueous or organic solvents and the solutes are often pharmaceutical [2, 3] or nutraceutical [4] compounds.

Changing such operating parameters as pressure and temperature, drying temperature, and solute concentration has an appreciable effect on particle size and morphology. So, too, does changing the length-to-diameter ratio of the restrictor. However, the parameter most important to engineering the size of particles is the ratio of the flow rates of the solution and the carbon dioxide.

Unfortunately, several of the operating parameters are intertwined and changing one may provoke a change in another one, or more. At a given operating pressure, for example, a relatively minor change in solution flow rate may have a profound effect on the solution - CO₂ ratio because it also brings about a change in the thermophysical properties of the fluid in the restrictor and a qualitative change in the flow pattern.

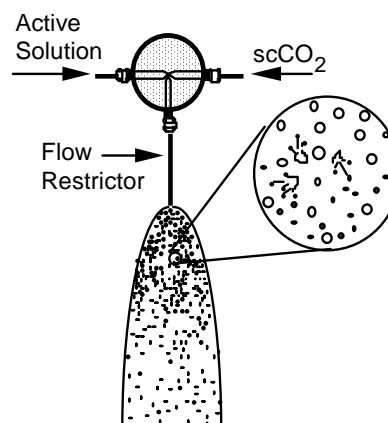


Figure 1. Illustration of CAN-BD nebulization and droplet formation.

As the solutions and the carbon dioxide are each relatively insoluble in one another, the fluid flowing through the capillary is a very complex emulsion that may consist of three phases — liquid and vapor CO₂, and the liquid phase pharmaceutical solution — depending on where in the capillary the expansion decreases pressure below the CO₂ vapor pressure. If thermodynamic equilibrium is achieved within the capillary, solid phases of CO₂ and the solution are also conceivable as temperature and pressure expand below the triple point.

The literature is rich with experiments describing the flow of emulsions, or of multi-phase species, by researchers motivated by the needs of the petroleum or refrigeration industries. For the most part, they have in common a search for the frictional pressure gradient or the effective viscosity of the fluid under consideration. One example of a well-known work treating petroleum oil-water emulsions is Alvarado and Marsden's [5] experiments with macroemulsions flowing through tubes and porous media. These experiments, like most others pertaining to petroleum production or separation, involve incompressible fluids in a low- pressure environment far less than 1 MPa.

In contrast, the flashing of refrigerants in capillaries and other control devices was the subject of experiments by Melo, et al. [6] and by Lin et al. [7] who actually measured the pressure distribution along the length of a capillary through which R-12 was flowing. A notable observation was expansion of the fluid to its vapor pressure followed by further expansion along the saturation curve. For a thorough treatment of multiphase flows, we refer the reader to the recent text by Brennan [8].

Viscosity is obviously key to controlling the dynamics and thermodynamics of fluid processes within capillary flow restrictors, although there is not much in the literature that is particularly germane to CAN-BD nebulization due to the critical or near-critical operating pressures and the compressibility of carbon dioxide. This paper discusses the

results of a three-part experimental investigation of CO₂ – water mixtures flowing through long capillaries ($650 < L/D < 2500$) at inlet pressures greater than 7 MPa.

EXPERIMENTAL APPARATUS

We used the apparatus sketched in Figure 2 to complete the experiments. Two 500 ml syringe pumps (ISCO Model 280 D) fed either pure water (Purelab Option from Elga) or carbon dioxide (Local supplier), respectively, at predetermined pressures to separate ports of a mixing cross (Valco, part No. ZX1C). The CO₂ – water mixed flow was directed into synthetic fused silica flow restrictors of nominal internal diameters between 75 and 200 microns (Polymicro Technologies TSP series) that had been cut to predetermined lengths and fit to the third port of the mixing cross. A digital pressure transducer (Mensor Corp., series 6000) was attached to the fourth and final port of the cross. For the single specie experiments using either water or carbon dioxide alone, the mixing cross was replaced with a three-port mixing tee (Valco, part No. MT1XCS6).

Control systems on the Isco syringe pumps provide data on the volumetric flow rate and operating pressure of the pump but not the mass flow rate or density of the fluid. To calculate mass flow rate, a thermocouple was immersed in the carbon dioxide stream at the pump exit to record T_P , the pump exit temperature. Using the pump pressure, P_P , and T_P , we calculated the density of CO₂ at the pump exit and then, together with the indicated volumetric flow rate, computed the mass flow rate of carbon dioxide. Approximately one meter of 1/8TH inch diameter high-pressure stainless steel tubing

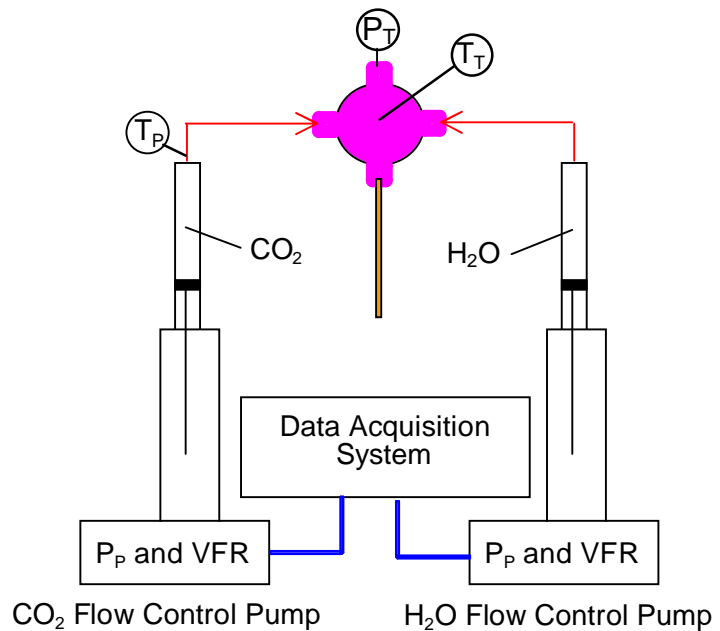


Figure 2. Schematic diagram of experimental apparatus.

directed the CO₂ from the pump to the mixing tee or cross. This line was not insulated and usually provided ample opportunity for the CO₂ to equilibrate to room temperature. Absent leaks (which are obvious due to frosting at the point of leakage), we thereby determined the mass flow rate of carbon dioxide into and through the mixing tee or cross.

A surface contact chromel-alumel thermocouple (Omega SA1XL-K-SRTC) was attached to an exterior surface to estimate temperatures of the fluids within the tee or cross. This is called tee temperature, T_T , and was rarely very different from the ambient laboratory temperature. Signals from the thermocouples, the pump control systems, and the mixing tee pressure transducer were sampled at a rate of 1/sec and recorded by a data acquisition system coded on a LabView platform.

Experimental Procedure

Prior to running each experiment, a record was made of the temperature, barometric pressure, and relative humidity in the laboratory. Mixing tees and crosses were attached to a lab stand positioned within a fume hood. All fittings and lines were checked for leaks which, if found, were repaired. Calibrations of gages were verified and assurance was made that the data acquisition system was properly functioning.

Single specie, water or carbon dioxide: The goal was to measure the flow rate of the specie at pressures between 3.5 MPa and 13.5 MPa through restrictors of different nominal geometries and use the data as volume fraction boundary conditions for the subsequent emulsion experiments. In separate tests, the fluids were pumped through each capillary restrictor beginning, typically, at a pressure of 3.5 MPa and then increased in increments of 1.4 MPa, approximately. Real time data were graphically displayed on the screen of a computer and clearly indicated when equilibrium had been achieved. For the water experiments this rarely exceeded 30 seconds but extended to 1 – 2 minutes when using the more compressible carbon dioxide. Upon reaching equilibrium, data were acquired for 1 – 2 minutes before the pressure was advanced to the next level. Data files were converted to Excel formats for later analysis before the next capillary was connected to the mixing tee.

Two species, water and carbon dioxide. After completing the lab preliminaries discussed above, CO₂ was pumped through the first restrictor at 6.9 MPa while water was simultaneously pumped to the mixing cross at 0.1 ml/min. When the flow had stabilized after approximately two minutes, data were recorded and the water flow rate was then increased to 0.2 ml/min. Water flow rates of 0.3, 0.5, 1.0, 2.0, 3.0, 4.0, and 5.0 ml/min were also used. This procedure was repeated for five additional operating pressures up to 13.5 MPa, approximately.

EXPERIMENTAL RESULTS

Pure Water Experiments

At room temperature and at pressures between 3.5 and 13.5 MPa, the changes in either water density or viscosity, and their ratio, is less than 0.5 percent. Our experiments with pure water flowing through a dozen, or so, capillaries defined approximately by $700 \leq L/D \leq 2500$ confirmed the relative constancy of water's properties throughout the range of pressures of interest. Thermophysical properties of pure fluids were calculated with REFPROP Version 8.0 [9] using measured temperatures and pressures as inputs. As expected, throughout the entire experimental range of pressures, the pure water experiments conformed to the Hagan-Poiseuille relationship, $\lambda = 64/RN$, at Reynolds Numbers (RN) up to around 2,000 as well as to Churchill's [10] equation for smooth capillaries up through $RN = 10,000$ and above.

Pure Carbon Dioxide Experiments

It is evident in Figure 3 that the mass flow rate of pure carbon dioxide varies almost linearly with pressure in the mixing tee. This is the case for every capillary in each family identified by its nominal internal diameter (ID). In this regard, the trends of the data resemble those that might be seen for the flow rate of a choked, isentropic compressible

fluid, but calculations made using the isentropic assumption with carbon dioxide failed to match our experimental data. As might be expected, for a given capillary length (L), mass

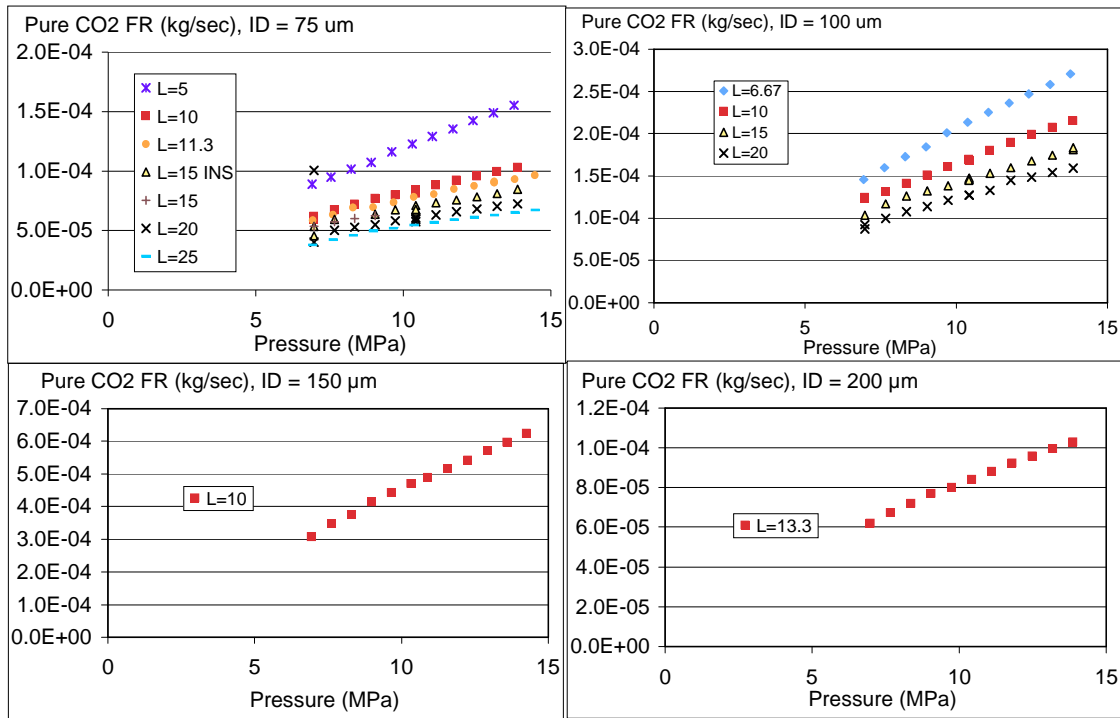


Figure 3. Mass flow rate of pure CO₂ through capillaries of various lengths, L (cm), with internal diameters of 75, 100, 150, and 200 μm as sheet parameters.

flow rate increases with internal diameter and, for a given internal diameter, mass flow rate decreases with increasing capillary length.

In one experiment we explored the effect of heat loss or gain, if any, through the capillary wall. This was accomplished with the ID = 75 μm, $L = 15$ cm flow restrictor and running the experiment once with the capillary insulated (INS, in Figure 3), and again without insulation. There are no apparent differences in the mass flow rate data for each experiment and it is therefore reasonable to assume that thermodynamic processes within the capillary may be considered adiabatic.

We attempted to correlate these data using notions from compressible fluid dynamics to the exclusion of viscous effects. This is shown in Figure 4 where the fit to the data is given by

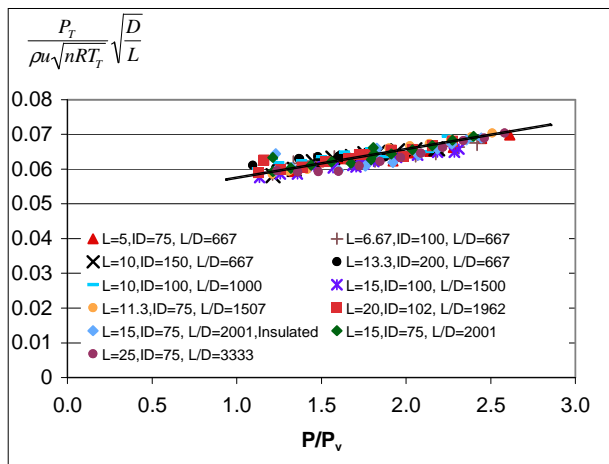


Figure 4. Correlation of data from pure CO₂ experiments run at nearly room temperature and $7 \leq P/P_v \leq 14$ MPa, eleven long capillaries described by $667 \leq L/D \leq 3333$.

$$\frac{P_T}{\rho u \sqrt{nRT_T}} \sqrt{\frac{D}{L}} = 0.0515 + 0.0072 \frac{P}{P_v} \quad (1)$$

Explicit viscous effects are presumably found within the coefficients, but the consistency of the correlation among so many L/D configurations suggests the pure carbon dioxide flow is governed as much by compressibility as by viscosity and, in particular, that under the conditions of our experiments, the flow is choked. Equation 1 may be rearranged to provide a convenient expression for the mass flow per unit area (ρu) in terms of the dimensions of the capillary and thermodynamic conditions in the mixing tee.

Water and Carbon Dioxide Experiments

With fixed values of pressure and temperature in the mixing tee it is intuitively obvious that increasing the flow rate of water will bring about a reduction in the flow rate of carbon dioxide. Examples of this behavior can be seen in Figure 5 for two different families of $L = 10$ cm capillaries, $ID = 75$ and $150 \mu\text{m}$. The chart on the left examines partitioning of the species through the entire range of CO_2 volume fractions, $0 \leq \phi \leq 1$, while the chart on the right provides data from experiments that concentrated more on the range $0 \leq \text{H}_2\text{O FR} \leq 1.0$, or $\phi \sim 0.8$ to 0.9 . The latter conditions are more representative of what is normally seen in CAN-BD experiments.

What appears to be an anomaly in the right chart of Figure 5 is understandable. Note that the data indicate that the CO_2 flow rates for $P_T = 8.3$ MPa are out of sequence with those obtained with $P_T = 7.0$ MPa and $P_T = 9.9$ MPa. A review of the file for these data indicates that we conducted the experiment immediately after filling the carbon dioxide pump and increasing its pressure to slightly more than 8.3 MPa. Compressing fluid in the syringe

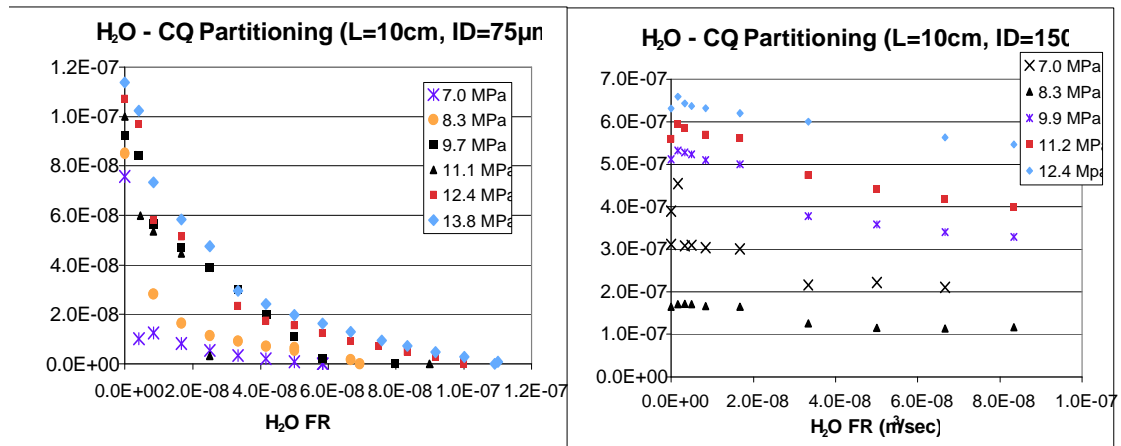


Figure 5. Partitioning of water and carbon dioxide flowing through $L=10$ cm and $ID = 75$ (left) or $150 \mu\text{m}$ (right) capillaries at constant tee pressure.

pump also raises its temperature and, in this case, we recorded tee temperatures near 40°C . Carbon dioxide at 8.3 MPa and 40°C is supercritical, data from all of the other experiments listed in Figure 5 were completed with carbon dioxide in the liquid state at the pump.

DISCUSSION OF EXPERIMENTAL RESULTS

Together with the appropriate conservation equations, the experimental results discussed in the previous section may be used to develop an implicit understanding of processes that take place within the capillary. The general features of these processes may be seen in Figure 6 where the fluid enters the capillary from the left with properties that we measured or deduced within the mixing tee. Expansion occurs first with the carbon dioxide in a liquid state but the decreasing pressure eventually reaches the saturation vapor pressure at some distance downstream, L_L , where the flow may then become mixed vapor and liquid. The flow finally exits the capillary at L where the pressure is the greater of atmospheric or critical (in the sense of choked flow, not the pressure at the critical point).

Integration of the equations of motion are more often used to predict thermodynamic and fluid dynamic properties of flows but, in this case, we choose to use our experimentally measured properties as initial conditions that lead to flow developments at various locations within the capillary. Our analysis makes certain assumptions, not the least of which is thermo-dynamic equilibrium throughout the flow field. In practice, fluid will pass through the capillary in 3 – 5 msec, so questioning if properties equilibrate is certainly

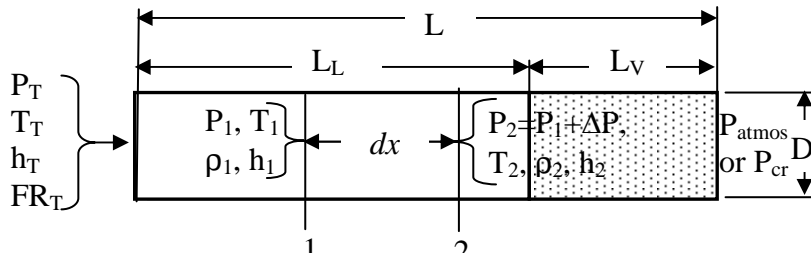


Figure 6. Schematic representation of capillary internal diameter, D , length, L , length of liquid flow, L_L , length of mixed or vapor flow, L_V , and element used for integration scheme.

appropriate. As fused silica has a thermal conductivity akin to brick, or $1/300^{\text{TH}}$ that of copper, heat transfer to or from the capillary walls is negligible and we assume the flow is adiabatic. This was verified with our experiment with an insulated capillary

(Figures 3 and 4). In view of the very brief time they are in contact, we neglect any transfer of heat between, or co-solvation of, the carbon dioxide and water. Finally, we assume the flow is homogeneous and that the velocities of all species and phases, liquids and vapor, should flashing occur, are equal. Homogeneity is a reasonable assumption for capillary flows as the difference between vapor and liquid phase velocities diminishes faster than \sqrt{D} and becomes zero when $D < 5$ mm [11]. Using the notation set forth in Figure 6, the respective conservation equations may be written as follows:

Conservation of mass

$$\frac{d\dot{m}_t}{dx} = \frac{d(\dot{m}_w + \dot{m}_c)}{dx} = 0 \quad (2)$$

Recalling that velocities of both species and their phases are all equal, leads to the definition of the average density at any position within the capillary,

$$\bar{\rho} = \rho_w \phi + \rho_c (1 - \phi) \quad (3)$$

so that the mass conservation equation may be written in a form that is more practical for integration

$$\frac{d(\bar{\rho}u)}{dx} = \frac{d}{dx} [\rho_w u \phi + \rho_c u (1 - \phi)] = 0 \quad (4)$$

As stated above, the results of our experiments with pure water indicate it is essentially incompressible over the range of conditions used in the experiments. Accordingly, in integrating the equations of motion, ρ_w is assumed not to vary along the capillary.

Conservation of momentum

The pressure gradient consists of contributions due to the acceleration of the flow through the capillary and to viscous forces:

$$\frac{dP}{dx} + \frac{dP_a}{dx} = \frac{dP_v}{dx} \quad (5)$$

where the contribution from acceleration may be written

$$\frac{dP_a}{dx} = \frac{d((\rho_w + \rho_c)u^2)}{dx} \quad (6)$$

while the viscous contribution is

$$\frac{dP_v}{dx} = \frac{1}{2} \bar{\rho} u^2 \lambda \frac{dx}{D} \quad (7)$$

Conservation of energy

$$\frac{d(h_w \phi + h_c (1 - \phi) + \frac{1}{2} u^2)}{dx} = 0 \quad (8)$$

We use Churchill's [10] universal friction factor, $\lambda = \lambda(\text{RN}, \varepsilon)$, valid for laminar and turbulent flows, in a step-wise and simultaneous numerical integration of equations (2) – (8). We assume that the roughness factor is negligible, $\varepsilon = 0$, for fused silica capillaries. Thermophysical properties were calculated using REFPROP v.8 [9] including the vapor quality, Q , of the carbon dioxide. Whenever $Q > 0$, we computed viscosity of carbon dioxide with the relationship attributed to McAdams *et al.* [12]

$$\frac{1}{\mu_c} = \frac{Q}{\mu_v} + \frac{1-Q}{\mu_l} \quad (9)$$

where subscripts l and v indicate liquid and vapor phases, respectively, and Q is the vapor quality. A number of authors have determined that the McAdams model of viscosity provides the best fit to experimental data obtained with a variety of refrigerants [7, 13,14].

The viscosity of the two-species flows was calculated by power series expansions in ϕ around the continuous phase viscosity. Thus, for $0 \leq \phi \leq 0.5$,

$$\mu = \mu_c \left(1 + \frac{5}{2} \phi\right) \quad (10)$$

Otherwise, for $\phi > 0.5$,

$$\mu = \mu_w \left(1 + \frac{5}{2}(1 - \phi) - 2(1 - \phi)^2 - \frac{1}{2}(1 - \phi)^3\right) \quad (11)$$

These expressions recover Einstein's [15] equation (*i.e.*, Equation (10)) for the viscosity of dilute emulsions near both $\phi = 0$ and $\phi = 1$ and, at intermediate values of ϕ , produces values of viscosity that considerably exceed those of either pure water or pure carbon dioxide.

We followed a traditional approach to integrating equations (2) through (8) step-by-step in that properties at station 1 in the current step were those at station 2 in the previous step. u_2 was determined via Equation (4) based on an initial estimate of $\bar{\rho}_2$, which we then subject to iteration to balance Equation (8). We selected a step size $dx = 0.05$ cm and reduced it to 0.005 cm in the event pressure in the restrictor passed below 1.0 MPa because it has been observed that temperature and pressure gradients may become large as x approaches L . At the entrance to the capillary, $x = 0$, we set the pressure, temperature, and flow rate that we measured in the laboratory and watched their evolution as the integration stepped along the capillary with increasing values of x .

Single specie experiments with pure carbon dioxide

The pressure at the end of the restrictor, P_L , should either be atmospheric pressure, or a critical pressure if the flow is choked. Figure 4 and equation (1) suggest that flow choking is likely. Moreover, the existence of atmospheric pressure at $x = L$ poses a problem because it is less than the triple point pressure of carbon dioxide and, therefore, transcends the calculation domain of REFPROP. Theoretically, if the flow were truly in thermodynamic equilibrium, one could expect to see solid phase carbon dioxide (flakes of dry ice) expelled from the end of the capillary. While we have never seen this in the laboratory, we regularly see flakes of dry ice form in the plume within a few millimeters of the capillary exit plane. We choose instead to assume that once beyond the triple point, the fluid exists as superheated liquid with properties determined by trend analysis of the preceding three steps, until atmospheric pressure has been achieved. We recognize weakness in this approach, but we also recognize that the scores of integrations we have completed rarely reach triple point pressures, but when they do, it is within ten, or so, steps of the capillary exit plane. The overall effect of the weakness cannot be substantial, especially since our calculations show that the flow usually chokes at a pressure considerably above atmospheric.

Figure 7 illustrates two particular results from stepwise integration of equations 3 – 8 using the McAdams model of viscosity, equation (8), for an $L/D = 2000$ capillary with two different experimental inlet conditions. The panels in Figure 7 describe distributions

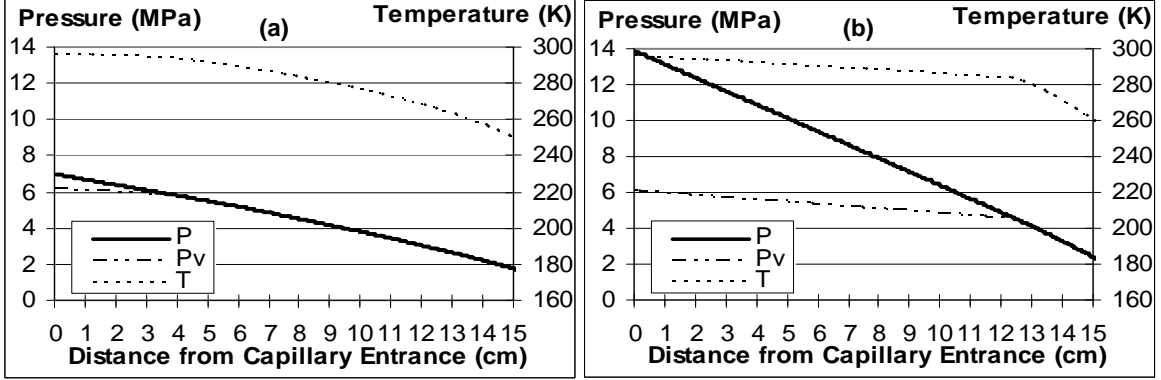


Figure 7. Calculations of pure CO₂ flow through a L/D = 1500 capillary with L = 15 cm and D = 100 μm. For panel (a), T_T = 296 K, P_T = 7 MPa, and VFR = 1.35 × 10⁻⁷ m³/sec. For panel (b), T_T = 296 K, P_T = 13.9 MPa, and VFR = 2.08 × 10⁻⁷ m³/sec.

of pressure, P, temperature, T, and saturation pressure, P_v, along the length of the capillaries. In every case we examined, pressure at first decreases almost linearly to the position (the liquid length, L_L, in Figure 6) where it equals the saturation pressure. Between the inlet, x = 0, and L_L, temperature decreases very little, although the distribution is also nearly linear. The saturation pressure also decreases in a linear fashion in the range 0 ≤ x ≤ L_L simply due to the small variation in temperature around 300 K. For positions in the capillary greater than L_L the distributions of pressure and saturation pressure are nearly coincident. This interesting feature has been observed and discussed before, notably by Lin *et al.* [7]. In neither panel of Figure 7 does the pressure reach atmospheric pressure, approximately 0.069 MPa, at the 15 cm exit of the capillaries. The flow is obviously choked.

The linear features of the pressure and temperature distributions discussed in connection with Figure 7 permit evaluation of L_L, the pressure at this position, and demonstration of the importance of this dimension on overall development of the flow of near critical carbon dioxide through adiabatic capillaries. Near the entrance to the capillary, the pressure gradient may be found from equation (7) when it is recognized (and confirmed by our calculations) that u₂ = u₁ to a close approximation. Thus, $\Delta P = q_T \lambda_T \frac{\Delta x}{D}$. Our calculations

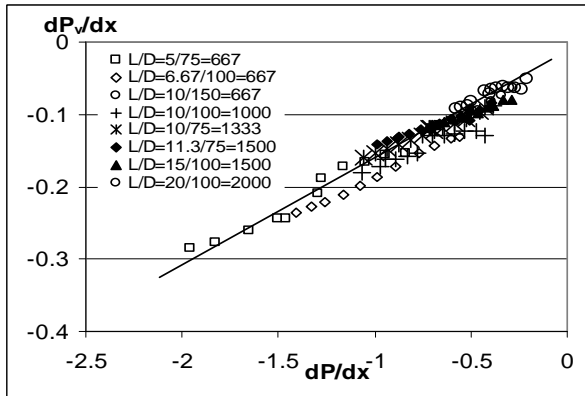


Figure 8. Dependence near the capillary entrance of the calculated saturation pressure gradient.

also provide the gradient of saturation pressure at the capillary entrance, $\frac{dP_v}{dx}$. Examples are shown in Figure 8 for eight different capillaries driven by tee pressures in the range 7 ≤ P_T ≤ 14 MPa.

When examined closely, the data presented in the figure show a weak dependence on the L/D ratio of each capillary. (In this and subsequent figures where data are identified by the L/D notation, L is in cm and D is in microns. The evaluated ratio is dimensionally

correct.) However the line shown in the figure and given by equation (12) estimates the calculated values of dP_v/dx reasonably well and may be used for algebraic calculations of L_L and P_L .

$$\frac{dP_v}{dx} = 0.0144 \frac{dP}{dx} - 0.02 \quad (12)$$

Pressure and saturation pressure are equal at L_L and by equating the two it can be shown that

$$L_L = \frac{P_T - P_{vT}}{\frac{dP_v}{dx} - \frac{dP}{dx}} \quad (13)$$

so the pressure, P_L , at the liquid length becomes

$$P_L = P_T + \frac{dP}{dx} L_L \quad (14)$$

Experiments with carbon dioxide and water

Figure 9 describes the calculated pressure and temperature distributions along the length of a capillary with $L = 10$ cm and $ID = 150 \mu\text{m}$ when water is flowing together with carbon dioxide. The volumetric water fraction is $\phi = 0.029$ for the left panel and $\phi = 0.066$ for the right panel. The three variables, P , P_v , and T , shown in the figure decrease in an almost

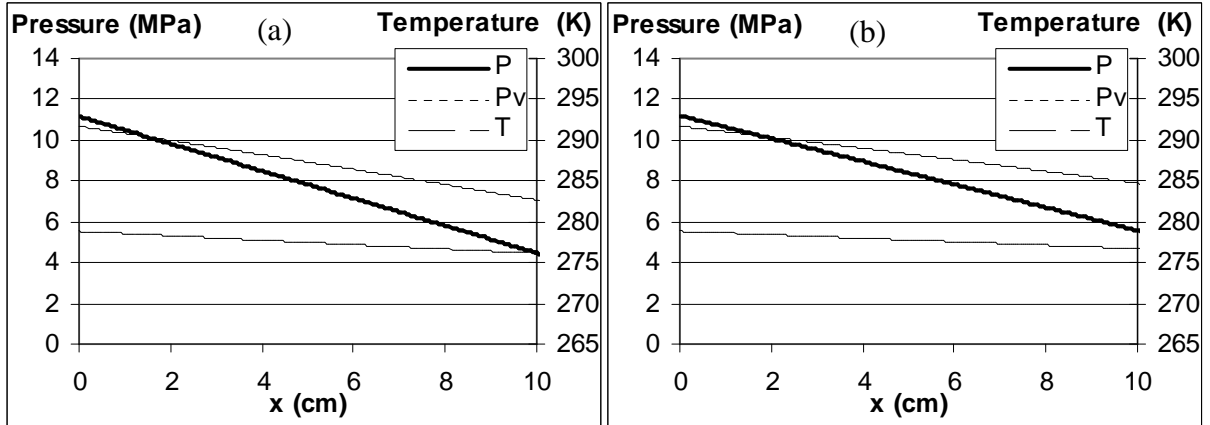


Figure 9. Pressure distribution along a capillary with $P_T = 11.2$ MPa. $L/D = 667$ with $L=10$ cm and $D=150\mu\text{m}$. $\phi = 0.029$ (a) and $\phi=0.066$ (b), respectively.

linear fashion and qualitatively resemble the distributions shown in Figure 7 for pure carbon dioxide. A notable difference, however, is that the length of the liquid region consumes the entire length of the capillary and, for the higher water fraction, appears to extend beyond the exit plane of the capillary where it presumably flashes abruptly to atmospheric pressure. For the tee conditions we examined, all of our calculations for this capillary show this feature: at or below a critical volume fraction, approximately $\phi = 0.03$, the liquid length is equal to or very slightly less than the capillary length. At volume fractions greater than critical, the emulsion expelled across the exit plane is in an entirely liquid state.

In Figure 10 we plot our experimental data for this capillary as specific total mass flow, or total mass flow (water + carbon dioxide) per unit area, against volume fraction of water. We have added a broken line to indicate the approximate locus of the critical volume fraction as determined by calculations akin to those presented in Figure 9. To the left of the broken line the liquid length lies within the capillary. To the right, the liquid length appears to extend beyond the capillary. Whether ϕ is greater or less than the critical volume fraction has a pronounced effect on specific total mass flow.

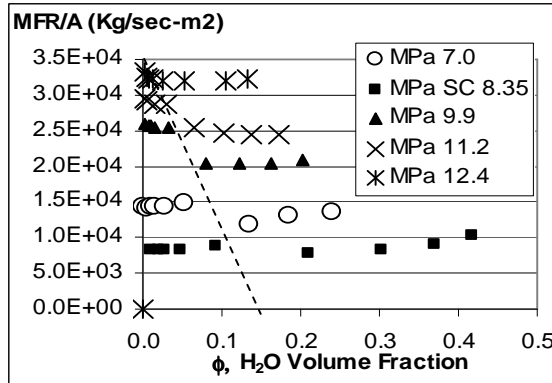


Figure 10. Total mass flow rate per unit area through an L/D=1500 capillary with L = 10cm and D = 150 μ m.

We direct attention to the 8.35 MPa data in the figure and, as previously discussed in connection with Figure 5, note that the properties of emulsions made with supercritical carbon dioxide are significantly different from those made with liquid CO₂, and, in this case, decrease expected flow rates by a factor of two, approximately. We suspect that reduced interfacial tension between water and supercritical CO₂ results in dispersed phase globules of a different size and, consequently, an emulsion with very different rheological properties.

When the water volume fraction exceeds 0.27, approximately, the emulsion appears to behave like a low Reynolds Number laminar flow. This is evident in Figure 11 where we plot the experimentally determined friction factor, λ_{calc} , against Reynolds number. For this purpose,

$$\lambda_{calc} = \frac{P_T - P_{amb}}{q_T} \frac{D}{L} \quad (15)$$

and the Reynolds Number were calculated using density and viscosity coefficient given by equations (3) and (11), respectively. The data lie on or about Poiseuille's equation which supports the notion of laminar flow. In contrast, when ϕ is less than 0.3, the flow is dominated by carbon dioxide with corresponding Reynolds Numbers of 10,000 or more, and the flow structure is turbulent.

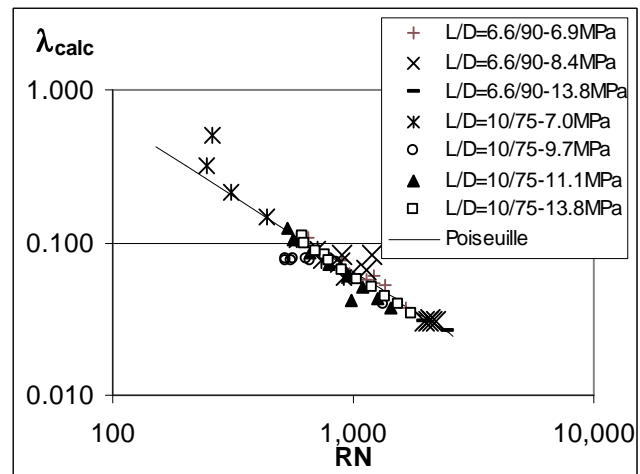


Figure 11. Values of the friction factor determined from experimental data.

CONCLUSIONS

Pure water flowing through long capillaries, $L/D > 650$, behaves as an incompressible fluid even at pressures approaching 14 MPa. In contrast, the high-pressure flow of pure carbon dioxide through capillaries with diameters between 75 and 200 microns is entirely different, with Reynolds Numbers exceeding 10,000 at pressures between 7 and 14 MPa. The flow is choked, with the exit pressure related to the length within the capillary that pressure remains greater than saturated vapor pressure, *i.e.*, with carbon dioxide in the liquid state. Throughout the liquid length the pressure gradient is nearly constant and may be accurately calculated by ignoring the acceleration of the flow and considering only viscous forces, equation (7).

When an emulsion of water and carbon dioxide is considered, the situation becomes more complex and is sensitive to the volumetric fraction of water, ϕ . Whenever ϕ is less than 0.1, approximately, total mass flow rates differ little from those of pure carbon dioxide under similar conditions of temperature and pressure in the mixing tee. But more often than not, the mixing length consumes the entire length of the capillary. There is a critical value of ϕ that varies in an unspecified manner with pressure at which the specific mass flow rate decreases abruptly to what appears to be a meta-stable intermediate condition that is a prelude to a Poiseuille-like laminar flow regime. Depending on pressure, this occurs at values of ϕ around 0.05 to 0.2 with the laminar regime occurring at $\phi \sim 0.3 - 0.5$.

SYMBOLS

Latin

| | |
|---|--|
| D (μm) | Internal diameter of capillary |
| FR (kg/sec or m ³ /sec as indicated) | Flow rate |
| h (kJ/kg) | Specific enthalpy |
| L (cm) | Length of capillary |
| P (MPa) | Pressure |
| Q | Vapor quality of vapor – liquid mixed flow |
| T (K) | Temperature |
| u (m/sec) | Velocity |

Greek

| | |
|-----------------------------|---------------------------|
| λ | Friction factor |
| μ (Pa-sec) | Coefficient of viscosity |
| ρ (kg/m ³) | Density |
| ϕ | Volumetric water fraction |

Subscripts

| | |
|------|---|
| amb | Ambient conditions |
| c | Carbon dioxide |
| calc | Calculated from experimental observations |
| L | Evaluated at the mixing length |
| T | Evaluated in the mixing tee |
| t | Total, as in total mass |
| V | Saturated vapor |

REFERENCES

- [1] SIEVERS, R.E., and KARST, U., U.S. Patent 5,639,441, **1997**.
- [2] SIEVERS, R.E., HUANG, E.T.S., VILLA, J.A., ENGLING, G., and BRAUER, P.R., J. Supercritical Fluids, 26, p. 9, **2003**.
- [3] CAPE, S.P., VILLA, J.A., HUANG, E.T.S., YANG, T.-H., CARPENTER, J.F., and SIEVERS, R.E. Pharm. Res., 25, p. 1967, **2008**.
- [4] PATHAK, P., QUINN, B.P., KRANK, D.M., BHAGWAT, P., McADAMS, D.H., REBITS, L.G., and SIEVERS, R.E., Pub 279, 239TH ACS Natl. Mtg. and Expo., San Francisco, CA, 2010.
- [5] ALVARADO, D.A. and MARSDEN JR., S.S., SPE Journal, 19, p. 369, **1979**.
- [6] MELO, C., NETO, C.B., and SILVA FERREIRA, R.T. DA, Trans. ASHRAE An. Mtg., Seattle, 105 Part 2, **1999**.
- [7] LIN, S., KWOK, C.C.K., LI, R.-Y., CHEN, Z.-H., and CHEN, Z.-Y., Int. J. Multiphase Flow, 17, p. 95, **1991**.
- [8] BRENNAN, C.E., Cambridge University Press, **2005**. (Also available at <http://caltechbook.library.caltech.edu/51/1/multiph.htm>)
- [9] LEMMON, E.W., HUBER, M.L., and McLINDEN, M.O., *NIST Reference fluid thermodynamic and transport properties – REFPROP. Version 8.0*. April, **2007**.
- [10] CHURCHILL, S.W, Chem. Eng. 84, p. 91, **1977**.
- [11] ZHAO, T.S. and BI, Q.C., Int. J. Heat and Mass Trans., 44, p. 2523, **2001**.
- [12] McADAMS, W.H., WOOD, R.L., and BRYAN, R.L., Trans. ASME, 64, p. 193, **1942**.
- [13] CHANDRA, B. and PRABHU, S.V., AIAA 2004-168, Reno, NV, January **2004**.
- [14] BITTLE, R.R. and PATE, M.B. ASHRAE Trans., 102(2), p. 52, **1996**.
- [15] EINSTEIN, A., Ann. Phys., 19, p. 289, **1906**

ACKNOWLEDGEMENT

The authors gratefully acknowledge the financial support of the U.S. Department of Agriculture's SBIR program.